ELSEVIER

Contents lists available at ScienceDirect

Marine Chemistry

journal homepage: www.elsevier.com/locate/marchem





Estimating benthic Fe and reactive solute fluxes

R.C. Aller*, I.P. Dwyer, D.A. Swenson Perger, C. Heilbrun, N. Volkenborn, L.M. Wehrmann

School of Marine and Atmospheric Sciences, Stony Brook University, Stony Brook 11794-5000, NY, USA

ARTICLE INFO

Keywords:
Benthic dissolved Fe flux
Early diagenesis of Fe
Marine Fe cycle
Benthic chamber design

ABSTRACT

The flux of dissolved Fe (Fe_d) from sediments is a critical component of the biogeochemical Fe cycle. Common approaches to estimating these fluxes are based on modeling of Fe_d porewater profiles or incubating sediment and overlying water using benthic chambers or retrieved cores. Inadequate resolution of pore water Fe profiles in the uppermost mm of sediments and rapid Fe²⁺oxidation can greatly compromise these approaches. These limitations may be partially responsible for large variations in reported benthic Fed fluxes at given values of independent controlling variables such as sedimentary Corg remineralization rates. A series of laboratory experiments were conducted to compare methods to estimate \overline{F} e fluxes and confirmed that \overline{F} e 2 is oxidized to \overline{F} e $^{3+}$ within a few minutes in oxygenated chamber water. The resulting ${\rm Fe}^{3+}$ colloids do not pass through 0.2 μm pore size filters and are also rapidly lost from suspension. Loss from suspension is partially reversible. Most benthic chamber studies do not correct for such losses and likely significantly underestimate Fed fluxes. Additional reactive components such as P and trace metals that associate with precipitated Fe-oxides must be subject to similar major losses during flux measurements. We modified the standard incubation methods by circulating overlying water through Fe extractors and accumulating Fe_d released into chambers over a known period at constant O₂ and pH. We found using a range of experimental conditions that in cylindrical chambers ~70-93% of introduced Fe²⁺ is typically recovered on accumulators at saturated O₂ (\sim 270 μ M) and seawater pH (\sim 8; NBS). We recommend that flux incubations that target reactive solutes (e.g., Fe, P) be configured with flow-through extractors, and pre-calibrated for losses specific to chamber designs, chamber water residence times, and deployment conditions (e.g., O2, pH).

1. Introduction

The release of dissolved iron (Fe_d; Table 1) from the seabed into overlying water is a fundamental step in the redistribution of sedimentary Fe in the oceans, and contributes substantially to its bioavailability. The potential for release is determined predominantly by diagenetic mobilization of Fe_d^{2+} , which is controlled by dissimilatory reduction of Fe-oxides (DIR) and the oxidation of Fe-sulfides in lithogenic sediments (e.g., Thamdrup, 2000; Raiswell and Canfield, 2012; Nielsen and Risgaard-Petersen, 2015). Both of these primary reaction pathways and their source strength are directly correlated with labile organic C supply ($C_{\rm org}$), benthic $C_{\rm org}$ remineralization rates, bottom water O_2 , and the magnitudes of reactive solid-phase Fe pools. Non-reductive remobilization of Fe_d is also believed to occur, although it is generally of lesser importance than DIR (Homoky et al., 2021). The transport of diagenetically mobilized Fe_d out of sediment defines the benthic Fe_d flux, and it is determined by balances between molecular diffusion, advection,

physical reworking, bioturbation (particle mixing, bioirrigation), and the consumption of Fe_d²⁺ during authigenic mineral formation (e.g., sulfides, carbonates, clays) or its oxidation to Fe³⁺ and reprecipitation within deposits. The latter is a function of overlying water O₂ and pH as well as Corg remineralization rates, all of which determine transport reaction scaling near the sediment-water interface and Fed flux into overlying water (Sundby et al., 1986; Thamdrup et al., 1994; Elrod et al., 2004; Sell and Morse, 2006; Lohan and Bruland, 2008; Severmann et al., 2010). Once released into oxygenated overlying water (or pore water), Fe_d^{2+} is rapidly oxidized to colloidal Fe-oxides, which in turn are scavenged by larger particles or transported laterally (Murray and Gill, 1978; Ussher et al., 2007). Organically chelated Fe³⁺ and Fe²⁺ in colloidal forms can also diffuse directly into overlying water, coagulate or be otherwise scavenged (Taillefert et al., 2000, 2007; Jones et al., 2011). The successive serial deposition, diagenetic remobilization, reoxidation, and transport in the water column can result in episodic migration of Fe within depositional basins, and its eventual burial as authigenic

E-mail address: robert.aller@stonybrook.edu (R.C. Aller).

^{*} Corresponding author.

Table 1Fe species definitions.

Fe Species	Definition
Fe _d	Fe that passes a $0.2~\mu m$ pore size filter (includes soluble (sFe) and colloidal (cFe) Fe of Homoky, et al., (2021); and reactive organic chelates)
Fe _d ²⁺ Fe _d ³⁺	Fe _d species with Fe oxidation state (II)
Fe_d^{3+}	Fe _d species with Fe oxidation state (III)
ΣFe	Total unfiltered Fe, includes Fe _d , colloidal Fe-oxide aggregates in
2_	suspension, and other forms of particulate Fe (e.g., lithogenic clays)
ΣFe^{2+}	Total unfiltered Fe with Fe-oxidation state (II)
$\Sigma \mathrm{Fe^{3+}}$	Total unfiltered Fe with Fe-oxidation state (III)

minerals characteristic of the terminal locus (e.g., Krauskopf, 1957; Aller et al., 1986; Raiswell and Anderson, 2005; Lyons and Severmann, 2006; Raiswell and Canfield, 2012; Lenstra et al., 2021; Burdige and Komada, 2020).

There are 4 primary approaches to estimating or constraining the benthic flux of Fe_d: 1). Estimate the flux directly using initial rates of Fe_d concentration changes in water overlying retrieved sediment cores ex situ or within a closed benthic chamber in situ. 2). Calculate the theoretical flux across the sediment-water interface from 1 or 2- dimensional pore water concentration distributions by utilizing a transport model, most commonly Fick's First Law of diffusion, often modified to include terms intended to account for Fe_d oxidation and bioturbation (particle mixing; bioirrigation). 3). Estimate a maximum flux from measurements of Fe_d production rates in sediments at steady state. And, 4). Estimate the flux by relating Fed, through transport models, to a wellcharacterized tracer such as 224Ra in either sediment or overlying water. These approaches have been reviewed periodically and continue to be modified through technical advances (Berner, 1980; Reimers et al., 2001; John et al., 2012; Burdige, 2006; Severmann et al., 2010; Thibault de Chanvalon et al., 2017; Homoky et al., 2016; Shi et al., 2019). Each approach can have substantial uncertainties because of the high reactivity of Fed coupled with inadequate measurement techniques, inaccurate models, or unsteady conditions. Examples of inadequate constraints are the low resolution of Fe_d concentration gradients in pore waters along sediment-water boundaries, little realistic information on benthic community activity, episodic pulses of labile Corg delivery to the seabed, or rapid changes in overlying water oxygen concentration and pH. The uncertainties inherent in measuring benthic Fed fluxes, together with a lack of basic understanding of the controlling factors (e.g., bioturbation), are evident in the 1-4 orders of magnitude variation of reported measured Fe_d fluxes for any given value of an assumed independent variable such as Corg remineralization rate that governs fluxes (e.g., Elrod et al., 2004; Dale et al., 2015; Homoky et al., 2016).

Here we describe a simple modification of the isolated overlying water – chamber incubation method that can greatly improve the accuracy of estimates of benthic Fe_d fluxes, and similarly particle-reactive solutes, in many common depositional environments such as relatively quiescent muds and shelf sands. The modified method is based primarily on an inline extraction – Fe accumulator but also on explicit recognition and correction for Fe_d oxidation in solution and loss on surfaces of the incubation chambers. As we show, these latter corrections depend on the operational definitions used to define Fe_d and on the design of chambers. While these modifications can greatly improve the estimate of Fe_d flux in specific applications, there remain major depositional environments such as deltaic mobile muds and particular boundary conditions for which benthic incubation methods, diffusive flux calculations, and steady state diagenetic models are not applicable, and Fe_d fluxes must be otherwise constrained (Aller, 2004; Song et al., 2022).

2. Experimental approaches to Fed flux measurements

2.1. Classic overlying water incubation method

Flux chamber incubation measurements are typically carried out using the initial rate behavior of solute concentrations, C(t), in this instance Fe_d , in an isolated volume, V, of water overlying sediment of area A. It is normally assumed that the solute flux, J, from (or into) sediment is constant for the incubation period and that it imposes small but measureable, time dependent changes in C(t) (t = time). Ideally changes in C(t) do not significantly impact the sediment-water boundary condition. In such cases, assuming no reactions in the overlying water, the initial rate of concentration change is given by:

$$\frac{dC(t)}{dt} = \frac{AJ}{V} \tag{1}$$

Numerous investigators have used the resulting well-known linear approximation, $C(t) \propto J t$, for over 60 years to estimate the net benthic fluxes of multiple solutes including O2, ECO2, nutrients, halides, and alkaline earths in addition to Fe_d and trace metals (Fig. 1A) (e.g., Jahnke et al., 2005; Berelson et al., 2007; Glud, 2008). One recognized issue for redox sensitive solutes such as Fe_d (or Mn_d) is that as O_2 is depleted in overlying water, the release of Fed from sediment can change drastically because the O₂ penetration scaling below the sediment – water interface is unsteady and rapidly decreases, thus increasing the net value of J (e. g., Sundby et al., 1986; Sell and Morse, 2006). The oxidative loss of Fed from solution in overlying water can also be affected by decreasing O_2 , as can bioturbation rates, resulting overall in nonlinear increases of Fed with time (Severmann et al., 2010). Thus, the periods of Fed flux incubations are typically set to minimize O2 depletion and associated artifacts. Any changes in pH, which are usually ignored, further accentuate nonlinearity because of the second order dependence of oxidation on [OH-] (Eq. (2)).

2.2. Modifications for reactivity and loss

It is possible to correct for oxidative loss of Fe_d in overlying water during flux incubations, the exact correction depending on the operational definitions of Fe_d and chamber design that are used, for example, Fe_d^{2+} only, $Fe_d^{2+,3+}$ combined, or $Fe_d^{2+,3+}+$ colloidal $Fe\ (=Fe_d)$. Each operational definition utilizes specific size cutoffs for filtration or different analytical method, and thus loss terms from an analytical window can differ. In the case of Fe_d^{2+} , the oxidation of Fe_d^{2+} to Fe_d^{3+} in seawater follows pseudo – first order kinetics with rate constant k, giving (Stumm and Lee, 1961; Millero et al., 1987; Pham and Waite, 2008):

$$\frac{dFe_d^{2+}}{dt} = -kFe_d^{2+} \tag{2}$$

where, $k \propto \frac{O_2}{(H^+)^2}$

The simplest correction for measures of J - Fe_d^{2+} using the behavior of C(t) during an incubation when O_2 , pH, and thus k are approximately constant, is then (Aller, 1980):

$$\frac{dC(t)}{dt} = \frac{AJ}{V} - kC(t) \tag{3}$$

Giving:
$$C(t) = C(0)e^{-kt} + \frac{AJ}{kV}(1 - e^{-kt})$$
 (4)

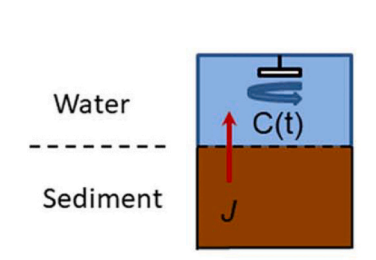
This relation predicts that a steady state concentration, C_{ss} , can be achieved in an incubation chamber such that:

$$J = \frac{VkC_{ss}}{A} \tag{5}$$

Example model predicted patterns for different removal rates are shown for a typical Fe_d flux of 200 μ mol m⁻² d⁻¹ in Fig. 2. Such steady behavior has been observed by Severmann et al. (2010) for filterable Fe_d

(A.) Closed chamber

(B.) Flow through chamber / extractor



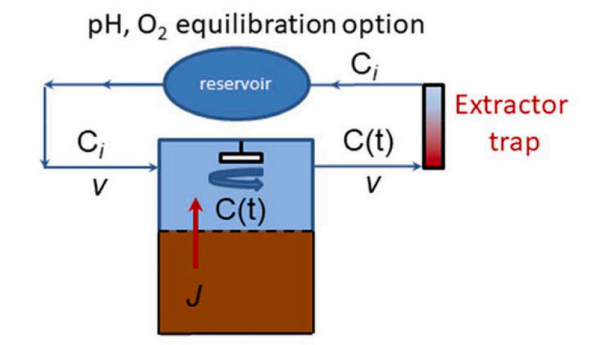


Fig. 1. (A). Schematic of typical closed chamber incubation with stirred, overlying water. (B). Flow through chamber with in-line extractor and equilibration reservoir.

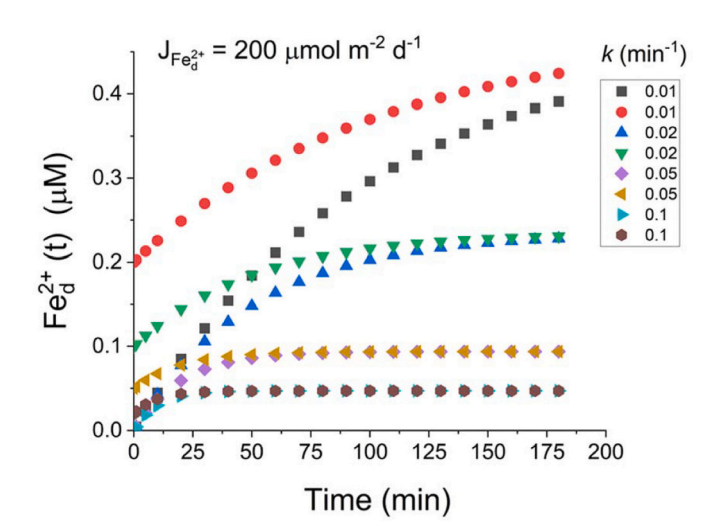


Fig. 2. Model predicted patterns of $Fe_d^{2+}(t)$ buildup in closed chamber at fixed $J_{\rm Fed}^{2+}=200~\mu{\rm mol}~m^{-2}~d^{-1};~A=167~cm^2,~V=1~L,$ and variable loss rate coefficients, k (e.g., oxidation; precipitation) (Eq. (5)).

(e.g., in their Fig. 3) but estimates of $J\text{-Fe}_d$ were not explicitly corrected on this basis to account for loss. Not accounting for oxidative loss of Fe_d can readily result in estimates of $J\text{-Fe}_d$ that are at least $10\times$ lower than actual Fe_d fluxes (Aller, 1980; Severmann et al., 2010). We further evaluate these losses below as they relate to different chamber designs, operation modes, and operational filtration steps (definitions of Fe_d; filtered and unfiltered).

2.3. An in-line extraction - Accumulator modification

We have modified the typical incubation chamber set-up to counter many of the oxidative loss terms for Fe_d, and to minimize the need for model corrections to flux estimates, although the modification does not entirely eliminate them (Fig. 1B). In this simple design, chamber water is continuously cycled through an extraction – Fe accumulator column which captures and removes Fe_d, before entering a reservoir that ensures specific O_2 concentrations (e.g., saturated O_2 or anoxic) and which can be used to largely stabilize pH. For example, reservoir aeration resaturates any depletion of O_2 and also strips excess CO_2 introduced from aerobic metabolism. We use glass wool as an inexpensive extraction medium that facilitates the oxidation of Fe_d^{2+} by atmospheric O_2 and efficiently removes Fe_0^{3+} - oxides across a broad size spectrum (e.g.,

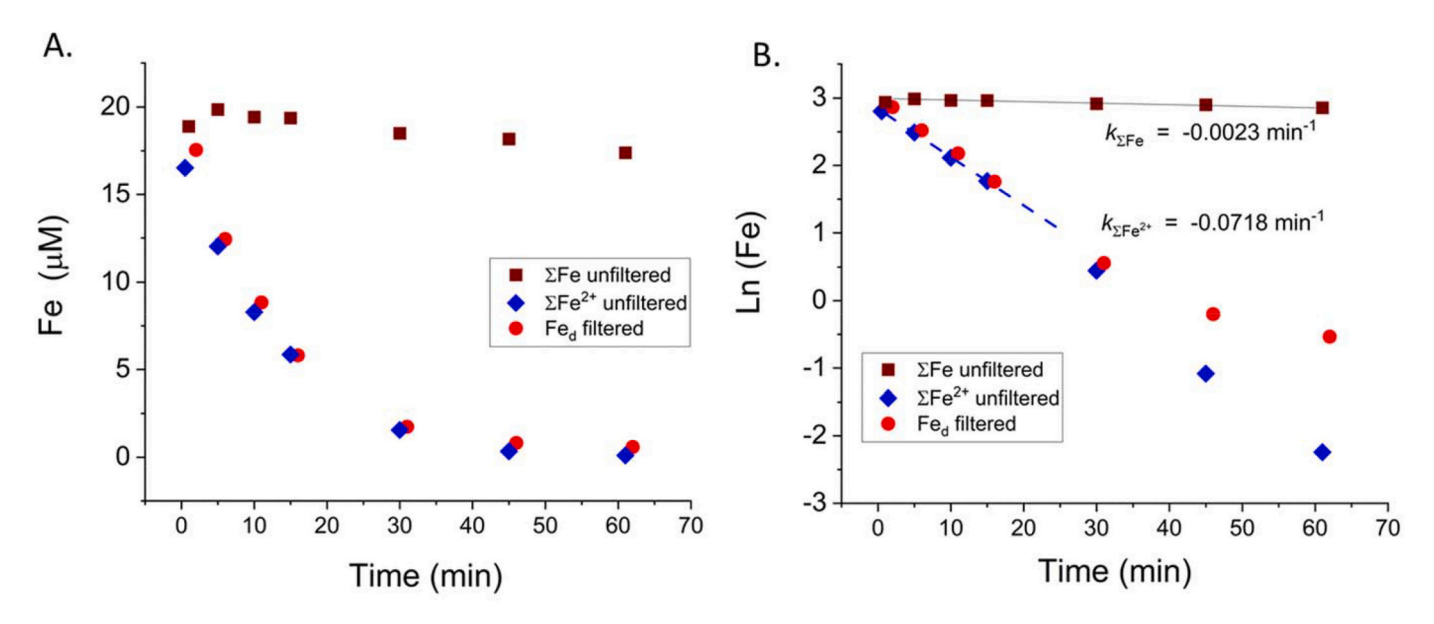


Fig. 3. (A) Behavior of dissolved Fe_d^{2+} , total filtered $ΣFe_d$, and total unfiltered ΣFe as a function of time in experimental run P2. (B) Ln(C(t)) plots illustrating periods of constant decay.

precipitation of Fe_d from solution; capture of particulate Σ Fe). Ion exchange resins targeting Fe_d²⁺, Fe_d³⁺, or other forms (e.g., organic chelated – Fe³⁺) and metals and not requiring oxygenated conditions can also be used. In this modification, water flows continuously at a rate, ν , out of the incubation chamber with concentration C(t), moves through an extraction - accumulator column, and then into a reservoir (optional), emerging with the concentration C_i and recycled into the incubation chamber (Figs. 1B, S1.1 – Supplement 1). The flow can be stopped, allowing the system to operate in the traditional incubation mode for short periods (Fig. 1A). The flux is calculated from the mass of diagenetically mobilized Fe extracted by the accumulator in a given time period divided by the sediment area. Loss of Fe onto chamber walls and tubing must also be accounted to derive the most accurate possible estimates. Assuming a constant flux, J, the modified relations between C (t), flow rate, and oxidative losses in the chamber are given by:

$$\frac{dC(t)}{dt} = \frac{A}{V}J - kC(t) - \frac{1}{\tau}\left(C(t) - C_i\right)$$
 (6)

where: v = flow velocity (volume/time)

 τ = overlying water residence time in chamber (V/v)

 C_i = input (recycled) concentration of reactive solute (often \sim 0) The expected concentration time dependence in chamber water is:

$$C(t) = C(0)e^{-\beta t} + \frac{1}{\beta} \left(\frac{C_i}{\tau} + \frac{AJ}{V}\right) \left(1 - e^{-\beta t}\right)$$
(7)

where: $\beta = (1/\tau + k)$.

A steady state concentration, C_{ss} can therefore be achieved such that:

$$J = \frac{V}{A} \left(\beta C_{ss} - \frac{C_i}{\tau} \right) \tag{8}$$

For many practical purposes, C_i is ~ 0 relative to C(t). It is important to realize that the value of k and the extraction column design must correspond to the targeted Fed species. For example, if the column extracts Fe_d^{2+} , Fe_d^{3+} , and colloidal - particulate Fe, then the value of k must reflect removal rates of total suspended Fe (= Σ Fe) within the chamber not simply the oxidative loss rate of Fe²⁺ to Fe³⁺. Assuming complete, irreversible removal of Σ Fe either in the chamber (with rate constant $k_{\Sigma E_0}$) and accumulator, then under steady conditions the fraction of the flux removed by the accumulator is: $1/\tau$ / ($k_{\Sigma Fe}+1/\tau$), and the fraction lost in the chamber is: $k_{\Sigma Fe}$ / ($k_{\Sigma Fe}$ + 1/ τ) (Supplement 2). Similarly, any unique behavior of organic - Fe complexes would need to be constrained. We show below example differences between these terms experimentally given typical operational definitions of Fe_d and Σ Fe. If there is significant lithogenic background relative to diagenetically mobilized Fe_d, a normalization scheme, e.g., ΣFe/Al, must be used. For example, if a significant diagenetic flux of Fed occurs with loss during oxidation from the Fe_d pool into ΣFe , the $\Sigma Fe/Al$ ratio should increase with time relative to the initial ratio or a crustal background ratio.

3. Methods

3.1. Experimental evaluation of Fe_d flux methods

We first determined that the behavior of Fe_d^{2+} in our experimental set-ups was consistent with reported kinetics of Fe_d^{2+} in seawater and with our operational definitions of Fe_d . We then evaluated the loss of Fe_d in two chamber designs and the efficiency of Fe_d extraction using accumulators and different operational modes. Finally, we compared the different incubation methods outlined previously to measure benthic Fe_d fluxes from natural sediments.

3.2. Fe_d^{2+} oxidation kinetics experiments

Seawater was collected at West Meadow Beach in central Long Island

Sound (LIS; salinity 25.5) and filtered (1 µm pore size). For an experimental run (labeled P series), 1 L of seawater was placed into a glass beaker open to air, continuously stirred on a magnetic stir plate with a teflon-coated magnetic stirring bar, and the temperature (T), pH, and O2 monitored. pH was measured on the NBS scale with a Vernier double junction wireless sensor. O2 and temperature were measured using Pyroscience FireSting fiber optic and thermistor probes, respectively. Following the procedure of Millero et al. (1987), we injected 20 µmol Fe_d^{2+} as $Fe(NH_4)_2(SO_4)_2$, and serially measured total filterable $Fe(\Sigma Fe_d)$, total unfiltered Fe^{2+} , and total unfiltered Fe (ΣFe). Stirring was unidirectional. Two 10 mL samples were removed, initially at 2-5 min intervals for 15-20 min, and subsequently 15-30 min intervals for a total of \sim 60–70 min, depending on the run. In each case, one 10 mL sample was immediately filtered through a 0.2 µm pore size polyethersulfonate inline syringe filter, the second was left unfiltered. Subsamples were immediately analyzed spectrophotometrically for Fe_d, Fe_d²⁺, ΣFe, or ΣFe²⁺ using Ferrozine with and without HONH₂·HCl reductant, respectively (Stookey, 1970; Viollier et al., 2000).

3.3. Chamber Fe_d oxidation kinetics and extractor calibration

Based on the results of the Fe_d^{2+} oxidation kinetics experiments, we determined the loss of Fe_d from solution and its behavior in two types of flux chambers; both were configured with in-line Fe extractors and equilibration reservoirs (Fig. 1B; S1.1 - Supplement 1). In each case, we injected a known quantity of Fe_d²⁺ (as Fe(NH₄)₂(SO₄)₂) into stirred chamber water sufficient for an initial Fe_d²⁺ concentration of \sim 20–100 μM ($\mu M = \mu mol L^{-1}$). Total unfiltered ΣFe and total filtered (0.2 μm pore size) Fed were measured in all chamber experiments as a function of time and incubation mode (flow or stopped flow). In a subset of cylindrical chamber experiments, filtered Fe_d²⁺ was also measured as a function of time. In most cases, the bottom of the chamber was PVC or polycarbonate (PC) but in two experimental runs, the bottom was acidcleaned, well-sorted, coarse quartz sand. Depending on the experimental run, the initial stages were: (1) continuous exchange, flowthrough mode with an in-line accumulator; (2) isolated chamber mode (stopped flow) for ~60 min followed by continuous exchange; and (3) isolated chamber mode (stopped flow) for ~120 min followed by continuous exchange. The stopped flow mode was comparable to conditions in most incubation data reported in the literature although for a shorter period than many field deployments. One type of incubation chamber was cylindrical, 14.6 cm ID, and held a water volume, V =1.8–1.9 L of seawater. One type was rectangular (5.4 cm width \times 12.8 cm length \times 2.9 cm tall; with volume of water V = 170-180 mL) and was designed for use with planar optodes. In all cases, LIS filtered (1 μm pore size) seawater was used. Chambers were connected using 0.64 cm ID PVC tubing to inline, glass wool extractors (2.0 \pm 0.1 g Pyrextm C3950, 8 µm diameter; loosely packed into 50 mL centrifuge tubes with pierced ends) and a reservoir which was constantly aerated with an air stone frit connected to an aquarium pump. The total seawater volumes in each system (chamber + reservoir) were \sim 4 L – 5 L (\pm 0.1 L). Flows through the chambers were maintained at a fixed rate (\sim 14–32 mL min⁻¹) with a peristaltic pump (Masterflex 7750). When flow was engaged, residence times of water were \sim 60–135 min in cylindrical chambers (1/ τ = 0.017–0.0075 $\text{min}^{-1})$ and 12–13 min in rectangular chambers (1/ $\!\tau=$ $0.08 \,\mathrm{min}^{-1}$). Glass wool in Σ Fe accumulators was dried and then leached for 7.5 h in 0.5 N trace metal grade HCl. Leachates were analyzed for total Fe using Ferrozine with HONH₂ · HCl. Glass wool was also leached separately in the same way to determine analytical background in leachates.

For cylindrical chambers, four experimental runs were carried out without a stopped-flow mode period (continuous exchange), two each with and without a bottom sand layer. All other runs incorporated an initial period of stopped flow time series sampling before initiating exchange: 4 runs for cylindrical chambers with ~60 min stopped flow; 4 runs for cylindrical chambers with ~120 min stopped flow; 2 runs for

rectangular chambers with $\sim\!30$ min stopped flow). For experiments with a stopped flow mode and time-series sampling of Fe_d, replicate experimental runs were carried out on separate days. Experimental series labeled FeJ4 employed continuous, unidirectional stirring in the chamber. Experimental series labeled FeJ10 employed bi-directional stirring in the sequence: 15 s clockwise; 15 s quiescent; 15 s counterclockwise; 15 s quiescent.

3.4. Sediment – Water exchange of natural sediments with and without using extractors

We used sets of cylindrical cores (14.6 cm ID; 27 cm height) to evaluate the extractor approach for natural sediments, and compare it to traditional isolated chamber and pore water concentration profile diffusion gradient methods. Sediment cores were collected (1/30/2021) from a sandy intertidal site located in southern Shinnecock Bay, Long Island, New York, close to the south end of Ponquogue Bridge. Cores were returned to the laboratory and sliced into depth intervals: 0-1 cm, 1-6 cm, and 6-15 cm. Sediment from each depth interval was combined in a bucket, homogenized for several minutes by hand using large plastic spoons, and sieved through a 5 mm mesh to remove large macrofauna and shells. The sediment was redistributed successively into 6 polycarbonate corer tubes, reconstituting the original relative depth distribution (6–15 cm basal layer; 1–6 cm middle; 0–1 cm top). These cores were configured in a recirculation system as in Fig. 1B (Fig. S1.3), with ~12 cm of overlying water and connected through a peristaltic pump to in-line extractors and a 4 L reservoir, which was constantly aerated. Three control chambers ~12 cm in height held water only and were otherwise setup identically to those containing sediment. Chambers held ~1.9 L of overlying water. Water used in this experiment was collected from the sampling site with a salinity 34. Temperature was 6 °C. Overlying water in the chambers for this experiment was stirred bidirectionally with magnetic stirring bars (~ 60 rpm; sequence as above) and recirculated at a rate 32 mL min⁻¹ (residence time ~ 1 h; Fig. 1B).

Three of the chambers containing sediment were further fitted individually with a water inlet tube set at a depth of 12 cm (3 cm from the base of core sediment), which was designed to simulate head-end injection during bioirrigation (Matsui et al., 2011). In the "irrigated" cases, overlying oxygenated water was introduced at $\sim\!12$ cm depth through 3 mm ID tubing repetitively with a pattern 10 min on (3.9 mL injection total =0.39 mL min $^{-1}$); 10 min off. This injection pattern simulated the winter irrigation volumes and frequency patterns of the maldanid polychaete, *Clymenella torquata*, common at the sediment collection site and is equivalent to $\sim\!10$ individuals / core or ~600 m $^{-2}$ (up to 2400 m $^{-2}$ is typically observed in the field) (Dwyer, et al., in prep).

The chambers were incubated with recirculation for 14 days (2/9/ 21–2/23/21) with changes of the in-line extractors every 1–2 days. On day 13, flow was stopped and time-series sampling of overlying chamber water done for measurement of O_2 uptake, filtered Fe_d , and unfiltered ΣFe . Water samples for Fe analyses were acidified with trace metal grade HNO_3 . Acidified samples were diluted 1:10 and analyzed at Rutgers University using inductively coupled mass spectroscopy (ICP-MS Neptune; CASS6, NASS7, In 2 ppb standards; detection limit $0.7~\mu M$).

On day 14, sediment pore water profiles were sampled using 5 cm long rhizons inserted radially through ports drilled at successive depths into the cylindrical tube walls (Seeberg-Elverfeldt et al., 2005; Steiner et al., 2018). Rhizon samples were acidified with trace metal grade HNO3, diluted 1:20 and analyzed in the FIRST Lab at Stony Brook University using inductively coupled mass spectroscopy (ICP-MS Agilent; detection limit 0.7 μ M). In addition, Fe optical sensors which allowed 2D imaging of Fe $_{\rm d}^{2+}$ concentrations (Zhu and Aller, 2012), were inserted vertically to depths of $\sim\!\!7-\!15$ cm to capture Fe $_{\rm d}^{2+}$ profiles across the radii of the cores. Optical sensors were calibrated with Fe $^{2+}$ solutions at 6 °C (detection limit $\sim\!\!2$ μ M at 20 min reaction time; Zhu and Aller, 2012). In order to correct the free solution calibration for sediment

diffusion properties, the depth-averaged absorbances between 8 and 10 cm were assumed to correspond to the concentrations measured by ICP-MS over the same intervals, and the concentration / absorbance ratio used to correct the free solution calibration slope.

4. Results

4.1. Fe_d^{2+} oxidation kinetics

Two experiments (P1, P2) were carried out on separate days, one over a pH range of 7.57–7.60 (mean: 7.57); T = 23.5-24.06 °C, (mean: 23.86); $O_2 = 272.8-274 \mu M$ (mean: 273.6); and a second over a pH range of 7.83–7.75 (mean: 7.75), T = 23.06-23.34 °C (mean: 23.19), O_2 = 274.6–277.6 μ M (mean:275.3). The NBS – Total [H⁺] scale offset of the pH electrodes used was 0.16 pH units (pH_T buffers per Dickson, 1993). Both experiments showed comparable behavior. The results from the second experiment at slightly higher pH (=7.75) are shown in Fig. 3. Fe_d^{2+} was rapidly oxidized with a rate constant of -0.0718 min^{-1} over the first ~ 30 min ($t_{1/2} = 9.7$ min), and at a slightly higher rate thereafter (Fig. 3). The total filtered Fe_d corresponded closely in concentration with total unfiltered ΣFe^{2+} , demonstrating that virtually all filtered Fe_d was Fe_d^{2+} , that is, very little Fe_d^{3+} , presumably as (nano) particulate Feoxide, passed the 0.2 µm pore size filter (Fig. 3). In contrast, the total unfiltered Σ Fe, only a small fraction of which was Σ Fe²⁺ after \sim 5–10 min, decreased approximately 30-times slower with a k = -0.0023 min^{-1} (t_{1/2} = 300 min). In the slightly lower pH case (pH = 7.57), Fe²⁺ decreased with a rate constant 0.0311 min⁻¹ over the initial 15 min, and the rate constant for unfiltered Σ Fe was -0.0006 min^{-1} . During oxidation, water turned progressively more yellow with time. The ratio of the average pH values (7.57 vs. 7.75) implies an oxidation rate ratio of 2.29 for Fe_d²⁺ in the two runs given the expected second order dependence in [H⁺] (Eq. (2)). The observed rate constant ratio is 2.31 (note: the ratio is independent of pH scale). The rate constant ratio for unfiltered Σ Fe, which reflects removal from suspension onto the container surfaces and not a chemical reaction per se, was 3.8. We did not investigate the possible pH dependence of removal from suspension (unfiltered Σ Fe) further.

4.2. Incubation chamber Fe_d oxidation kinetics and extractor calibration

In all chambers, filtered Fe d decreased exponentially within ${\sim}60\,\text{min}$ to near analytical background concentrations after Fe_d²⁺ tracer introduction (Figs. 4, 5). In the 4 cylindrical chamber cases (FeJ10) where time series Fe_d²⁺ were also measured, Fe_d²⁺ correlated closely with filtered Σ Fe (0.2 μ m pore size), comparable to glass beaker runs (Fig. 6). The corresponding rate constants for Fe_d^{2+} were -0.218 - 0.255 min⁻¹ for pH = 7.92–7.98 (Table 1). When rate constants in the chambers (polycarbonate) were ratioed to the values in the P1 and P2 (glass beaker) runs, they lie closely on a linear regression against the respective ratios of $[H^+]^2$ of the measurements, as expected from Eq. (2) if kinetics were controlled primarily by solution not container properties in both cases (O2 did not substantially differ). During individual runs, O2, pH, and T (temperature), varied around the mean values listed in Table 2 with standard deviations (SD) of 3 (μM), 0.03, and 0.3 (°C) respectively. In contrast to Fe_d²⁺ and Fe_d (filtered), the initial rates of decrease of total unfiltered Σ Fe were highly variable and $\sim 2–50\times$ lower (average \sim 14×) than k-Fe_d filtered. The concentrations of unfiltered Σ Fe were sometimes irregular after the period of rapid initial decrease, with both small increases, decreases, or relatively steady concentrations (Fig. 5). The recirculation concentrations \textit{C}_i were ~ 0.05 to 0.25 μM ; and ~ 10 - $100\times lower \, than \, the \, chamber \, water \, concentrations \, over the \, duration \, of$ the experiments (typically totally \sim 230-300 min). Depending on circulation conditions, the extractor columns in cylindrical chambers returned a net total accumulated ΣFe of 18.8 to 37.3 μmol out of 40 μmol injected, giving a range of recovery fractions of 0.47 to 0.93. (A glass wool background of 0.146 $\mu mol\,Fe$ was subtracted to obtain the net, i.e.,

R.C. Aller et al. Marine Chemistry 249 (2023) 104221

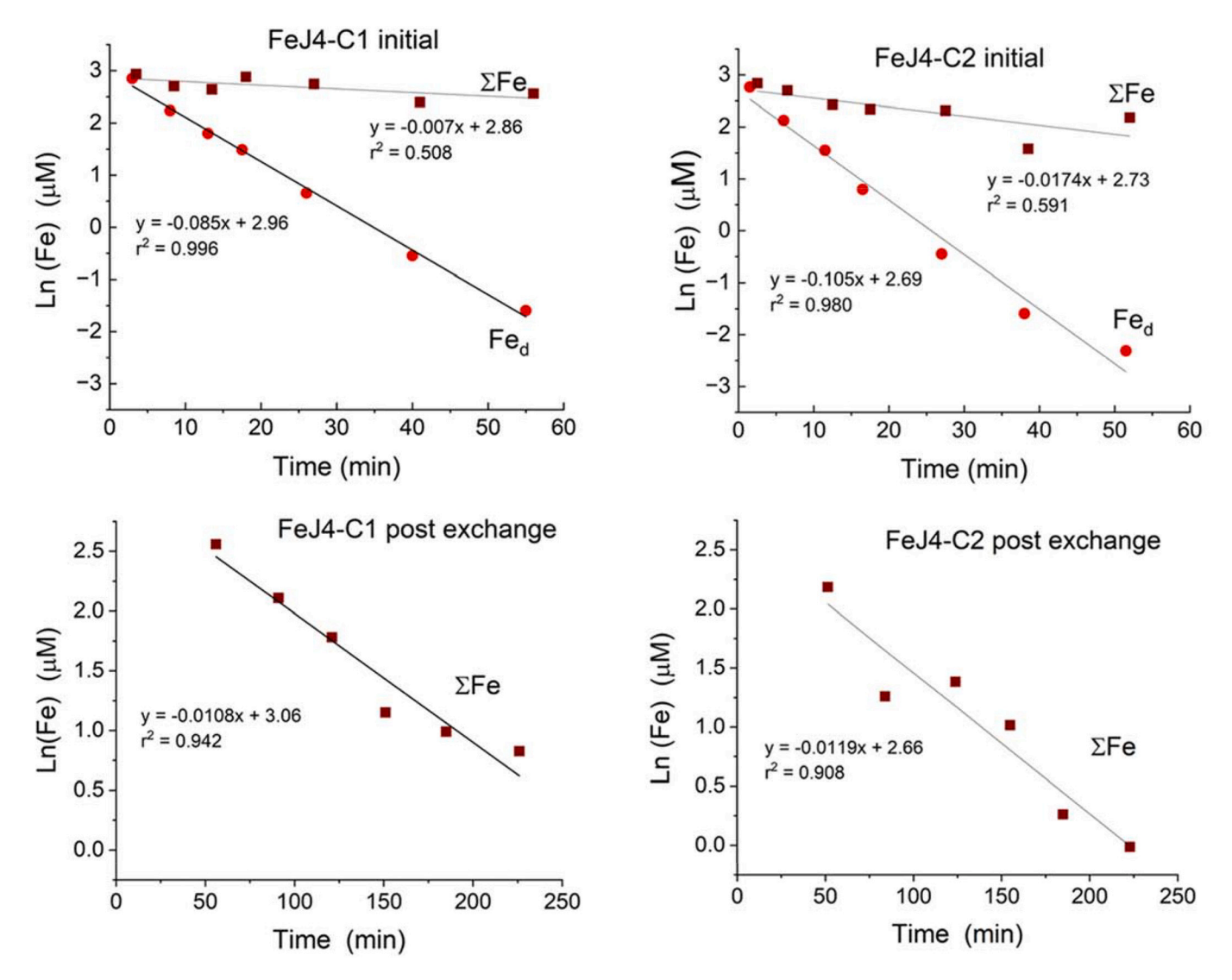


Fig. 4. Example Ln(C(t)) patterns of filtered Fe_d and unfiltered ΣFe in cylindrical chambers before (closed) and after exchange (circulation with reservoir).

glass wool $=0.0096~\mu mol~Fe~g^{-1}).$ The highest recoveries, averaging 0.89 ± 0.03 (i.e., 89% recovery) were obtained when circulation exchange was continuous during and following tracer injection (stopped mode =0 min). In these cases, the residence times were ~68 min, much longer than the characteristic half-lives of Fe_d^{2+} (2.7–3.2 min), ΣFe_d -filtered (2.8–3.3 min), and ΣFe_d -filtered (6–9 min; initial behavior) in the chamber water. When a stopped flow period of $\sim60-120$ min was used before initiating circulation (i.e., no filtered Fe^{2+} or ΣFe_d remaining; low unfiltered ΣFe_d , recovered fractions dropped to 0.47–0.715. The lowest recoveries were in cylindrical chambers that were stirred unidirectionally (FeJ4 series).

The rectangular, optocosm chambers (O1, O3) showed similar overall loss patterns to the cylindrical chambers but with significant quantitative differences. Although 3 separate runs were made, only data from O1 and O3 were retained for evaluation because of unstable pH (downward drift) in run O2 due to insufficient rinsing after acid cleaning of the system. For runs O1 and O3, filtered Σ Fe decreased exponentially during the first 25 min to near analytical background concentrations. The rate constants were -0.258 and -0.198 min $^{-1}$ (Table 2). Unfiltered Σ Fe removal had reaction rate constants -0.053 and -0.062 min during isolated chamber mode in O1 and O3, respectively. Following initiation of circulation and exchange, the recirculation concentrations C_i (reservoir concentrations) were below analytical detection up to ~ 0.4 μ M but predominantly 0.1-0.2 μ M, over the duration of

the experiments (~110 min). The post-exchange unfiltered ΣFe (total) decreased at rates -0.068 and $-0.06~min^{-1}$, analytically indistinguishable from the rate before exchange. In the relatively small, rectangular chambers, significant loss of unfiltered ΣFe occurred from the oxidized suspension, decreasing from ~38–70 μM to ~10–15 μM , before we initiated circulation through the Fe accumulators. The extractor columns in these cases returned a net total accumulated ΣFe of 3.26 and 2.58 μmol out of the 10 μmol injected for O1 and O3 respectively (~0.34–0.50 fractional recovery, correcting for Fe removal during sampling).

4.3. Sediment - Water fluxes with and without using extractors

The overlying chamber water (day 13) measured in two cores, nonirrigated core NG -5 and irrigated core IG -9, showed steady concentrations of both unfiltered suspended ΣFe and filtered ΣFe_d over the times of incubation (Fig. 7). Unfiltered ΣFe averaged 1.49 and 0.72 μM for irrigated and nonirrigated treatments, respectively. Filtered ΣFe_d averaged 0.06 and 0.01 μM for the irrigated and non-irrigated treatments, the latter not significantly above background. Pore water profiles of Fe²⁺in the same cores, radially averaged over $\sim \!\! 7$ cm at each pixel depth of the optical image, showed increases of Fe²⁺ with depth in both treatments but substantially lower average concentrations in the irrigated than nonirrigated treatment (Fig. 8). The vertical concentration

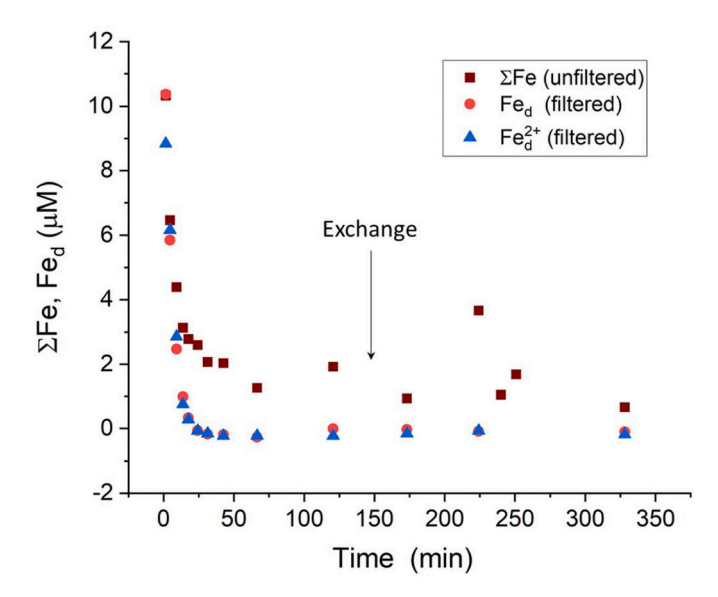


Fig. 5. Example Fe species as a function of time in cylindrical chamber FeJ10-

Unfiltered total Σ Fe comes to a relatively constant background >0 after \sim 1 h. The arrow marked "Exchange" indicates when flow out of the chamber and through the inline accumulator was initiated (128 min).

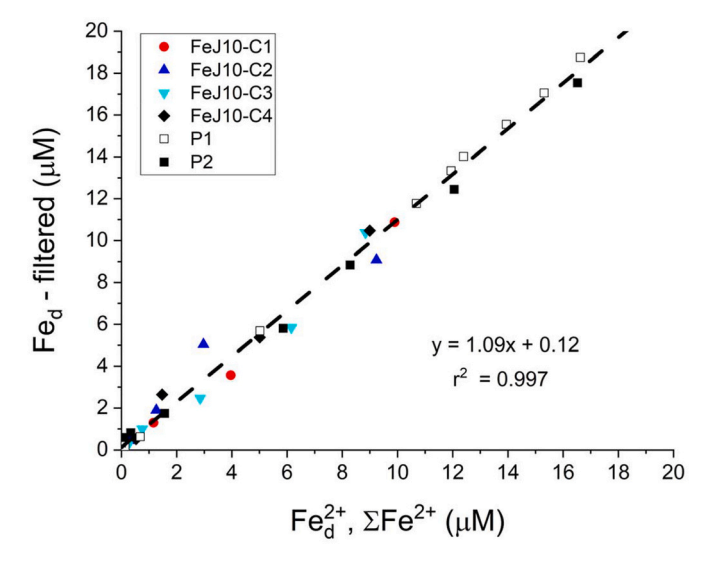


Fig. 6. Correlation of Fe_d^{2+} (FeJ10) or unfiltered ΣFe^{2+} (P1, P2) with total filtered Fe_d demonstrating close correspondence in multiple independent experimental runs. Virtually all Fe_d is Fe_d^{2+} .

gradient of Fe²⁺ based on optical sensor data over the upper ~ 1 cm was indistinguishable from 0. These gradients indicate a diffusive flux for Fe²⁺ of ~ 0 (not detectable). In contrast, the rhizon extracted pore water profiles of ΣFe_d for NG-5 and IG-9 showed detectable dissolved total Fe in the upper ~ 1 cm. The speciation of rhizon extracted ΣFe_d is unknown. The calculated concentration gradients assuming a linear extrapolation of concentrations from the rhizon depths to the sediment-water interface ($\Sigma Fe_d \sim 0$) are 183 and 171 nmol cm $^{-4}$ for the nonirrigated and irrigated treatments respectively. There are no reported measurements of colloidal Fe $^{3+}$ or chelated-Fe $^{3+}$ diffusion coefficients in sediments, so we utilize exclusively a free solution diffusion coefficient for Fe $^{2+}$ at 6 °C, salinity =30 of ~ 0.35 cm $^{-2}$ d $^{-1}$ to estimate fluxes from the concentration gradient. After correcting for tortuosity using the modified Weissberg relation and a porosity of $\phi=0.4$, we calculate a whole sediment

diffusion coefficient for Fe²⁺ of ~0.12 cm⁻² d⁻¹ (Boudreau, 1997). From Fick's First Law of diffusion (J = - ϕ D_s (∂ C/ ∂ z)), we further estimate possible diffusive fluxes (linear gradient) using the rhizon profiles of ~90 and 85 μ mol m⁻² d⁻¹ for the non-irrigated and irrigated cases.

We also utilized the relationship proposed by Raiswell and Anderson (2005) to roughly account for precipitation of Fe^{2+} within the oxidized sediment layer and the resulting nonlinear concentration gradients as the sediment – water interface is approached (after Boudreau and Scott, 1978). The flux, J, of Fe^{2+} into overlying water is given in this case by:

$$J = \frac{\varphi\sqrt{kD_s} C_{Fe}}{\sinh\left(\sqrt{\frac{k}{D_s}} L_{O_2}\right)}$$
 (9)

where $L_{O2}=$ the thickness of the oxygenated sediment layer, k= first-order removal rate constant; D_s is the diffusion coefficient of Fe_d^{2+} ; C_{Fe} the Fe^{2+} concentration at the base of the oxygenated layer. We assumed a pH ~ 7.5 ($k=\sim \!\! 0.085$ min $^{-1}$; Table 1); oxygenated layer thicknesses of $\sim \!\! 0.1-0.3$ cm (based on measured O_2 fluxes, overlying water O_2 and Cai and Sayles, 1996); and a basal C_{Fe} concentration at L_{O2} equal to the values measured in rhizon samples at $\sim \!\! 0.7-1$ cm (Fig. 8). The resulting flux estimates are 0.0007-35 and 0.0006-28 μmol m $^{-2}$ d $^{-1}$ for nonirrigated and irrigated cases ($L_{O2}=0.3-0.1$ cm).

The sediment ΣFe fluxes measured from the Fe accumulators over day 13 to 14 ranged from 2 to 14 μ mol m⁻² d⁻¹ in non-irrigated treatments (NG-5 = 14) and ~ 30 –52 μ mol m⁻² d⁻¹ in irrigated treatments (IG-9 = 52) (Fig. 9).

5. Discussion

5.1. Loss of Fed from solution and suspension

In our experiments, we confirmed the extremely rapid oxidation kinetics of Fe_d²⁺ in seawater under O₂ and pH conditions that are typically found in the overlying water during benthic chamber incubations. Although the role of O₂ concentration in overlying water during incubation is a critical control on the oxidation kinetics and net release of Fe_d^{2+} from sediment, the second order dependence of oxidative loss on [H⁺] means that even small excursions in pH (e.g., 0.1) during incubation can impact behavior of Fe_d²⁺. Fe_d²⁺ half-lives are a few minutes and, perhaps most critical for operational measures of Fed fluxes, most of the Fe_d³⁺ products, presumably Fe³⁺-oxide colloids, do not pass through a $0.2 \mu m$ pore size filter (Table 1; Fig. 6). There may also be larger colloidal particles (e.g., up to ${\sim}1~\mu\text{m};$ Raiswell and Canfield, 2012) that could be released from sediments similarly to Fe_d and not otherwise measured by common protocols. Thus, an operational filtration step in a measurement of Fe_d release in benthic chambers or incubated cores under oxic conditions must greatly underestimate Fed fluxes unless measurements are specifically corrected for loss from solution using a model such as Eq. (3). Similarly, any reactive component that strongly associates with suspended Fe³⁺-oxides, will likely also be lost from the analytical window during filtration, for example H₂PO₄ or trace metals. We did not evaluate the possible roles of other solutes such as Mn_d²⁺ released simultaneously from sediments in governing the phenomenological behavior of Fe_d²⁺ in incubation chambers. We note that our kinetic behavior studies may not exactly replicate conditions within chambers where multiple additional diagenetic reactions can occur.

The losses of Fe_d^{2+} from solution ($< 0.2~\mu m$) can be partially countered by simply utilizing total unfiltered ΣFe , rather than filtered Fe_d , as the analytical measure of Fe release. The total unfiltered ΣFe includes suspended Fe - oxides formed during oxidation of Fe_d^{2+} near the sediment –water interface or within the water column, as well as suspended lithogenic Fe. We found that the initial behavior of the suspended, unfiltered ΣFe formed after tracer introduction is also dominated by pseudo- first – order removal from suspension in glass beakers or incubation chambers but with rates that are $\sim 2-10\times$ slower than Fe_d^{2+}

Table 2 Summary results.

Run	Chamber type	Bottom	Stopped flow (min)	v (mL min ⁻¹)	τ (min)	T (°C)	pН	O ₂ (μΜ)	k-Fe _d ²⁺ min ⁻¹	k - Σ Fe _d (filtered) min ⁻¹	k - Σ Fe (unfiltered) min ⁻¹	Fe Injected (µmol)	Recover fraction
P1	Beaker	Glass	66	0	NA	23.9	7.57	274	-0.0311*	-0.0321	-0.0006	20	NA
P2	Beaker	Glass	62	0	NA	23.2	7.75	275	-0.0718*	-0.0778	-0.0023	20	NA
FeJ10- C1	Cyl.	PVC	130	27.3	68	22.1	7.92	261	-0.255	-0.209	-0.077	40	0.632
FeJ10- C2	Cyl.	PVC	125	27.3	68	22.2	7.98	263	-0.247	-0.226	-0.093	40	0.737
FeJ10- C3	Cyl.	PVC	128	27.3	68	22.3	7.97	264	-0.218	-0.208	-0.080	40	0.728
FeJ10- C4	Cyl.	PVC	123	27.3	68	24.2	7.94	261	-0.245	-0.248	-0.114	40	0.686
FeJ4- C1	Cyl.	PVC	59	13.7	135	25.5	7.55	257	-	-0.085	-0.007	40	0.542
FeJ4- C2	Cyl.	PVC	56	13.7	135	24.8	7.79	260	-	-0.105	-0.017	40	0.504
FeJ10- C5	Cyl.	sand	0	27.3	68	23.3	8.02	268	-	-	-	40	0.900
FeJ10- C6	Cyl.	PVC	0	27.3	68	22.6	8.01	269	-	-	-	40	0.933
FeJ10- C7	Cyl.	PVC	0	27.3	68	21.6	8.01	272	-	-	-	40	0.880
FeJ10- C8	Cyl.	sand	0	27.3	68	21.7	8.01	271	-	-	-	40	0.858
FeJ4- O1	Rect.	PC	36	13.7	12.4	25.3	7.55	251	-	-0.258	-0.3**	10	0.497
FeJ4- O3	Rect.	PC	26	13.7	13.3	24.9	7.74	254	-	-0.153	-0.062	10	0.337

^{*} unfiltered Fe²⁺; **Possible analytical error initial concentration unfiltered Σ Fe.

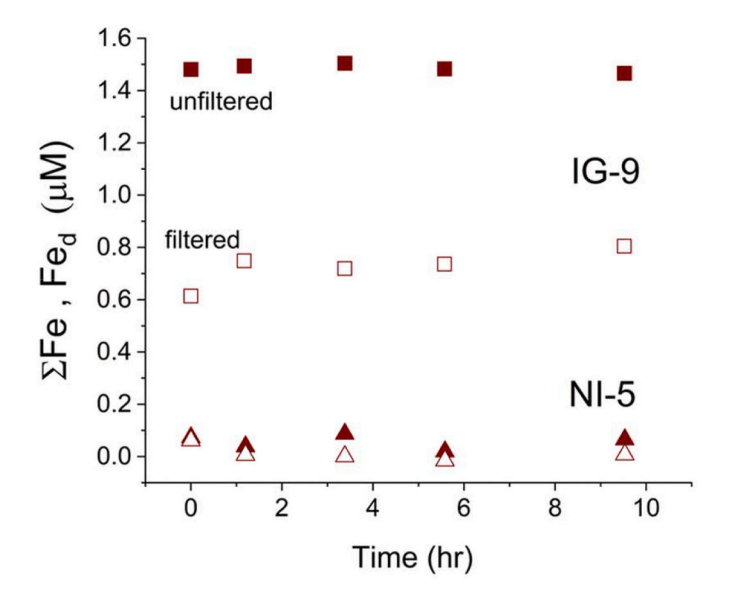


Fig. 7. Time series, stopped flow incubation of chamber water Fe_d (filtered) and ΣFe (unfiltered) for microcosms IG-9 (irrigated) and NI-5 (nonirrigated) (day 13). (ICP – MS analytical method).

oxidation rates (Table 2; Figs. 3, 5, 6). This initial behavior suggests that a first order removal rate model might also be a means of correcting measured build up patterns of unfiltered ΣFe for loss from suspension. However, the removal of suspended unfiltered ΣFe is not complete over the timescales of our experiments (2–5 h after tracer introduction), and typically approaches a steady background of $\sim\!1–2~\mu M$ (Fig. 5). This behavior suggests that removal of Fe^{3+} -oxides from suspension is not irreversible and that resuspension of Fe^{3+} flocs or desorption / detachment of colloidal Fe^{3+-} - oxides from chamber and tube surfaces are possible.

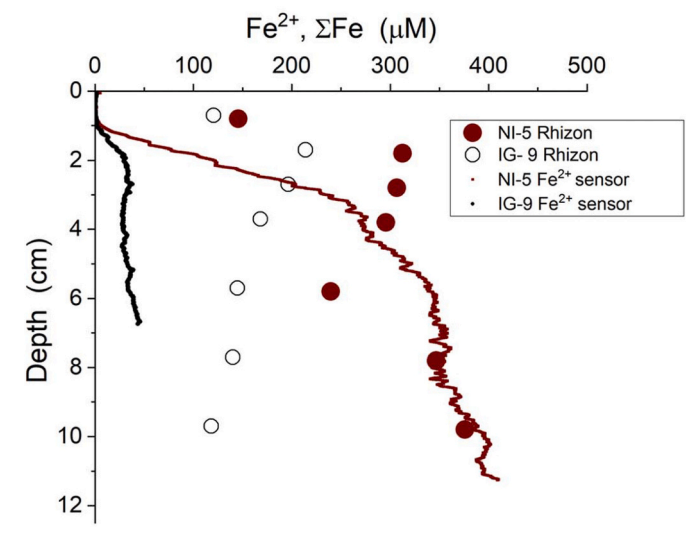


Fig. 8. Pore water profiles of Fe_d^{2+} (optical sensing foils) and Fe_d (rhizon) in NI-5 (nonirrigated) and IG-9 (irrigated) microcosms (day 14). Fe_d^{2+} profiles are radial averages from the axes to walls as a function of vertical depth in the cylindrical chambers.

5.2. Behavior of Fe accumulators

In our experiments with cylindrical chambers, the in-line Fe accumulators captured 50–90% of the Fe_d^{2+} tracer introduced into chamber water (Table 2). The highest yields (85–93%) were obtained when flow through the incubation chambers was continuous, that is, there was no extended stopped-flow period, and the water residence times within chambers were ~ 1 h. The lowest yields (50–54%) occurred when flow was stopped following the introduction of tracer and the residence times were ~ 2 h. When flow was stopped for $\sim 1-2$ h periods after tracer injection (i.e., to simulate a standard closed benthic chamber incubation

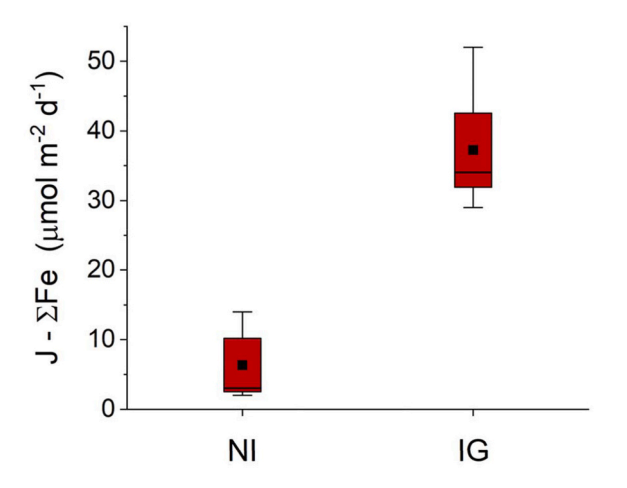


Fig. 9. Fe accumulator based fluxes determined for nonirrigated (n = 3) and irrigated treatments (n = 4) of natural sediment experiment JFe8 (day 13–14). Mean = square; median = line; range = whisker; SE = box.

period of several hours), a large fraction of the Fe_d^{2+} introduced at t =0 was removed from both solution and suspension within the chambers; for example, \sim 90–100% loss of $Fe_d^{2+},\,Fe_d,$ and ΣFe occurred before circulation exchange of chamber water was initiated in the case of run FeJ10 C3 (Fig. 5). Despite this apparent removal within chambers, most of the introduced Fe_d²⁺ was efficiently recovered on the accumulators. The presence or absence of sediment surfaces, at least sand, did not discernibly affect recovery, so trapping of flocs or adsorbed Fe on complex natural (granular) surfaces appears not to be a significant problem. The two runs with rectangular chambers suggest a lower overall efficiency of accumulator capture, perhaps reflecting more complex chamber circulation and stall areas (e.g., Tengberg et al., 1995). Overall, this behavior supports the conclusion that apparent removal of Σ Fe from suspension is at least partially reversible, that is, a large fraction of the precipitated Fe-oxide flocs or Fe^{3+} colloids adsorbed or otherwise attached to chamber surfaces can be released back into suspension and eventually scavenged by the Fe accumulators.

In principle, if the resuspension or desorption / detachment processes result in a stable, predictable concentration of unfiltered Σ Fe in suspension, C_{rs} , within a chamber system, then the kinetic relationships in the model Eqs. (3) to (5) formulated for unfiltered Σ Fe could, for example, be modified with an additional source term $k_{\Sigma Fe}C_{rs}$ (Supplement 3). This modification would result in a predicted steady state relation in chamber water of:

$$J_{\Sigma Fe} = \frac{Vk_{\Sigma Fe}(\Sigma Fe_{ss} - C_{rs})}{A} \tag{10}$$

The values of $k_{\Sigma Fe}$ and C_{rs} would need to be independently determined for each chamber system using the applicable operational definitions of ΣFe , concentration ranges, and conditions used. As shown by comparison of the steady state concentrations of unfiltered ΣFe (ΣFe_{ss}) in overlying water with the typical background concentrations due to desorption – resuspension measured in the tracer manipulations (Figs. 5, 9), the concentration differences (ΣFe_{ss} – C_{rs}) are likely very small and thus subject to very large uncertainties in practice.

Based on our results, the Fe accumulators represent a practical approach to measure Fe_d release from sediments relatively accurately without the need for phenomenological kinetic models or detailed consideration of the operational Fe speciation or specific desorption-resuspension behavior of a chamber system. Our experiments did not address the relative capture efficiency of ΣFe species such as organic complexes on the extraction media; however, we think that for most practical cases, the Fe-oxides formed or extracted within the accumulators should efficiently scavenge most forms of diagenetically released Fe, particularly after cycling of multiple chamber water volumes

through the accumulators.

5.3. Comparison of Fe flux estimate methods using natural sediment

The accumulator-based estimates of Fe_d fluxes measured in 3 nonirrigated and 4 irrigated microcosms demonstrated a distinctly higher net flux of Fe_d from sediment into overlying water in irrigated relative to non-irrigated treatments (Fig. 9; Supplemental Fig. S1.4). Although results are shown here only for the 13–14 day time bin to allow for comparison with the alternative methods of flux estimation at the same time (Table 3), this relative difference in Fe fluxes measured between the treatments (J_{Fe} irrigated $>> J_{Fe}$ - nonirrigated) was consistent at 10 separate sampling times throughout the 14 day experiment, and thus we are confident that these differences were not a one time excursion (Swenson, et al., in prep).

The time series overlying water Fe concentrations (day 14) indicated that steady state balances had been established between Fe fluxes and removal rates in the microcosms (Figs. 2; 7). Based on Eq. (5), the relative differences in fluxes in the respective treatments are simply the ratios of the steady concentrations, assuming that reaction rate constants for a specific operational form of Fe were the same in all chambers. The unfiltered and filtered concentrations were uniformly greater in the irrigated treatment than the nonirrigated treatment, and thus the relative concentrations are consistent with sustained higher J-Fed in irrigated relative to nonirrigated conditions. The relative concentrations of operational forms within treatments also showed that unfiltered ΣFe > filtered Fed, consistent with $k_{\Sigma Fe}\text{-unfiltered} < k_{Fed}$ filtered. The concentration ratios in IG-9 further imply k_{Fed} filtered / $k_{\Sigma Fe}$ unfiltered = 2.1 and in NG-5, the ratio = 4.7; also in the general ranges expected (e. g., Table 2). However, although the relative fluxes estimated from the concentrations have the expected relationships, the absolute magnitudes do not. For example, when an average value of $k_{\text{Fed}}\text{-filtered}$ of ${\sim}0.22$ min⁻¹ is inserted into Eq. (5) for IG-9 with a $C_{ss} = 0.72 \,\mu\text{M}$, unrealistically high J-Fe_d estimates >20 mmol m⁻² d⁻¹ result (Table 3). We do not know the reason(s) for such large discrepancies in the absolute magnitudes. It is possible, for example, that the forms of Fe_d released from the sediment had very different reactivity than Fe_d^{2+} (i.e., much smaller), or that not correcting for possible reversible adsorption or resuspension of suspended Fe within chambers (C_{rs}) results in large absolute errors using model corrections. As noted earlier (Eq. (10)), if the background concentration (desorbed or possibly chelated Fe_d) were of the same order as the measured C_{ss} , the required flux would be much smaller (e.g., \sim $100-200 \,\mu\text{mol m}^{-2}\,\text{d}^{-1}$). An advantage of the accumulators is that they obviate the necessity for specific model corrections.

The horizontally averaged pore water gradients of Fe_d^{2+} measured using planar optical sensors imply that there should have been virtually no detectable diffusive fluxes of Fe_d^{2+} into overlying water (Fig. 9). The

Flux estimate comparisons.

Treatment	Method	Flux (μ mol m ⁻² d ⁻¹)
NI-5	Accumulator	14
NI-5	Linear PW gradient (rhizon Fe _d)	90
NI-5	Nonlinear PW gradient (rhizon Fe_d ; L-O ₂ = 0.1–0.3 cm; pH 7.9)	0.0007-35
NI-5	PW gradient (Fe _d ⁺ ; optical sensor)	n.d.*
NI-5	k corrected OW (suspended ΣFe), Removal-only	900
NI-5	k corrected OW (Fe _d ²⁺), Removal-only	n.d.
IG-9	Accumulator	52
IG-9	Linear PW gradient (rhizon Fe _d)	85
IG-9	Nonlinear PW gradient (rhizon Fe_d ; L-O ₂ = 0.1–0.3 cm; pH 7.9)	0.0006–28
IG-9	PW gradient (Fe _d ²⁺ ; optical sensor)	n.d.
IG-9	k corrected OW (suspended ΣFe), Removal-only,	22,000
IG-9	k corrected OW (Fe _d ²⁺), Removal-only	28,000

^{*} n.d. = below detection.

images suggest, however, that there may have been upwards advection of pore water near the axes of the chambers (i.e., inner 2 cm; $\sim 10\%$ of chamber area) where concentrations of a few $\mu M\ Fe_d^{2+}$ are evident near the sediment-water interface (Fig. 10). The patterns also suggest slight downward advection along the chamber walls. Separate tracer experiments with fluorescein indicated, however, that given the stirring protocol, advection due to stirring should have been minimal. We cannot quantitatively evaluate such advective fluxes given our data, but the patterns are suggestive of areas of exchange that could support the ΣFe flux measured by the accumulators. The higher ΣFe fluxes in the irrigated treatments (Figs. 8, 9) are consistent with the sensor image for IG-9 that implies extensive flushing of sediment and advective release of Fed to overlying water (Fig. 10).

In contrast to the optical sensors, rhizon extracted pore water samples suggest high concentrations of Fed in the upper cm (centered on depth 0.7 cm) that might support both diffusive and advective fluxes. It is possible that these high concentrations represent organically complexed Fe³⁺ and as such were undetected by the optical sensors but not ICP-MS (Taillefert et al., 2000, 2007). It is also possible that advection of pore water during rhizon extractions resulted in artificially high Fe_d concentrations caused by upward movement of pore water during sampling. In any case, if we assume the concentrations are accurately assigned, we calculated (see Results) possible Fe_d fluxes of ~90 (nonirrigated) and ~ 85 (irrigated) μ mol m⁻² d⁻¹, by considering a linear concentration gradient extrapolated to the sediment-water interface (Table 3). These linear extrapolations do not allow for precipitation as the oxygenated interface is approached and are highly uncertain (Thamdrup, 2000). A common approach to address this issue is to try to account for oxidation of Fed in the oxygenated surface layer using a precipitation model dependent on the thickness of the oxidized layer (Eq. (9); Raiswell and Anderson, 2005; Homoky et al., 2012; Wehrmann et al., 2014). Corrections for precipitation within the oxygenated layer of sediment assuming a relationship such as Eq. (9) are crude at best, but they do indicate the major losses that must occur (Table 3) with values of 0.0007--35 and $0.0006\text{--}28~\mu\text{mol}~\text{m}^{-2}~\text{d}^{-1}$ for nonirrigated and irrigated experimental set-ups ($L_{\rm O2}=0.3$ –0.1 cm). There are sharp gradients in pH and O₂ near the sediment-water interface that are not explicitly taken into account in Eq. (9), and in addition, we have only estimates of homogeneous kinetic constants (Table 1) and not the heterogeneous kinetics typical of sedimentary porous media (e.g., Taylor, 1987).

The absolute and relative differences in Fe flux estimates derived using different methods illustrate the potential large uncertainties in constraining sedimentary Fe release patterns even under well controlled

laboratory settings (Table 3). The accumulators unambiguously revealed differences in Fed fluxes in response to sedimentary transport – reaction processes, in this case simulated bioirrigation, that might otherwise be very difficult to confidently resolve with model calculations or qualitative indicators such as relative pore water concentrations (Figs. 9,10; S1.4; Wehrmann et al., 2023). We think that our results confirm that overall, the use of in-line ΣFe accumulators provides the most straightforward, conceptually consistent, and accurate estimates of benthic Fed release that are the least affected by operational definitions of Fed or ΣFe species, and by model assumptions regarding transport – reaction conditions within sediments and the overlying water in chambers. Similar inferences apply to virtually any reactive component released from sediments.

6. Conclusions

The high reactivity of Fe_d in oxygenated seawater must be explicitly accounted for in benthic chamber based measurements of sedimentwater Fe_d fluxes. Exact corrections depend on operational definitions of Fe_d or suspended ΣFe , the system design, and system operation (e.g., chamber water stirring and residence times).

Reported benthic flux estimates of Fe_d that have not been explicitly corrected for Fe_d or oxidized product losses from solution (filtration losses) and suspension within chambers are likely inaccurate.

In principle, it is possible to correct observed Fe_d release patterns for nonconservative behavior using kinetic models of oxidation and precipitation. Model predicted patterns, for example, steady concentrations, have been observed in chambers in both the lab and field.

Benthic chamber systems used for Fe flux estimates should be calibrated to determine the behavior of Fe_d and suspended ΣFe given a particular system design, operational Fe pools, and chamber conditions (e.g., stirring patterns; residence times).

A simple modification to benthic chamber designs is to circulate chamber water continuously through in-line extractor columns that directly accumulate released Fe $_{\rm d}$ and oxidized products (e.g., colloidal Fe $^{3+}$), and also allow maintenance of fixed O $_{\rm 2}$ and pH conditions during flux incubations.

In-line Fe accumulators permit relatively accurate estimates of the net release of sedimentary Fe without specific assumptions regarding transport – reaction conditions within sediments and chamber water.

In principle, Fe accumulators should also be applicable for measurements of the fluxes of additional reactive constituents whose behavior is closely associated with that of Fe, for example, P, Ra, and

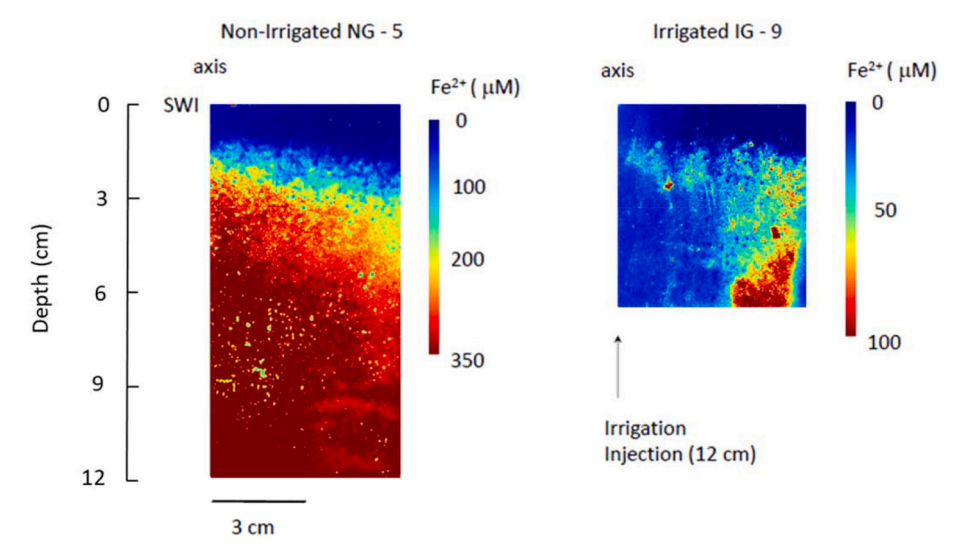


Fig. 10. Fe²⁺ concentration images extending from the cylindrical chamber axes to walls. There is a small radial gradient (a few μ M) toward the axial region, suggesting upward advection. Note pseudocolor scale differences for NI and IG.

other transition metals.

In-line extractors - accumulators should be adapted as a standard component of benthic flux chambers for both in situ and ex situ systems.

Declaration of Competing Interest

The authors declare no competing interests.

Data availability

Experimental data are available at NSF BCO-DMO data repository

Acknowledgements

This research was supported by NSF grant OCE 1757045 Chemical Oceanography Program. RCA, NV, LMW conceived the study. IPD and DAS collected field samples. IPD, RCA, CH, and DAS set up and carried out laboratory experiments and analyses. RCA wrote the manuscript first draft. All authors contributed to data interpretation, discussions, and edits of the manuscript. We thank D.J. Burdige and two anonymous reviewers for constructive critical comments that significantly improved the manuscript.

Appendix A. Supplementary data

Supplementary data to this article can be found online at https://doi.org/10.1016/j.marchem.2023.104221.

References

- Aller, R.C., 1980. Diagenetic processes near the sediment- water interface of Long Island sound, II: Iron and manganese. In: Saltzman, B. (Ed.), Advances in Geophysics. Academic Press, New York, USA, pp. 349–413.
- Aller, R.C., 2004. Conceptual models of early diagenetic processes: the muddy seafloor as an unsteady, batch reactor. J. Mar. Res. 62, 815–835.
- Aller, R.C., Mackin, J.E., Cox, R.T., 1986. Diagenesis of Fe and S in Amazon inner shelf muds - apparent dominance of Fe reduction and implications for the genesis of ironstones. Cont. Shelf Res. 6, 263–289.
- Berelson, W.M., Balch, W.M., Najjar, R., Feely, R.A., Sabine, C., Lee, K., 2007. Relating estimates of CaCO₃ production, export, and dissolution in the water column to measurements of CaCO₃ rain into sediment traps and dissolution on the sea floor: a revised global carbonate budget. Glob. Biogeochem. Cycles 21. https://doi.org/10.1029/2006GB002803. GB1024.
- Berner, R.A., 1980. Early Diagenesis A Theoretical Approach. Princeton University Press, Princeton.
- Boudreau, B.P., 1997. Diagenetic Models and their Implementation: Modelling Transport and Reactions in Aquatic Sediments. Springer-Verlag, Berlin.
- Boudreau, B.P., Scott, M.R., 1978. A model for the diffusion-controlled growth of deepsea manganese nodules. Am. J. Sci. 278, 903–929.
- Burdige, D.J., 2006. Geochemistry of Marine Sediments. Princeton University Press, Princeton.
- Burdige, D.J., Komada, T., 2020. Iron redox cycling, sediment resuspension and the role of sediments in low oxygen environments as sources of iron to the water column. Mar. Chem. 223, 103793.
- Cai, W.-J., Sayles, F.L., 1996. Oxygen penetration depths and fluxes in marine sediments. Mar. Chem. 52, 123–131.
- Dale, A.W., Nickelsen, L., Scholz, F., Hensen, C., Oschlies, A., Wallmann, K., 2015.
 A revised global estimate of dissolved iron fluxes from marine sediments. Glob.
 Biogeochem. Cycles 29, 691–707.
- Elrod, V.A., Berelson, W.M., Coale, K.H., Johnson, K.S., 2004. The flux of iron from continental shelf sediments: a missing source for global budgets. Geophys. Res. Lett. 31.
- Glud, R.N., 2008. Oxygen dynamics of marine sediments. Mar. Biol. Res. 4, 243–289.
 Homoky, W.B., Severmann, S., McManus, J., Berelson, W.M., Riedel, T.E., Statham, P.J.,
 Mills, R.A., 2012. Dissolved oxygen and suspended particles regulate the benthic flux of iron from continental margins. Mar. Chem. 134–135, 59–70.
- Homoky, W.B., Weber, T., Berelson, W.M., Conway, T.M., Henderson, G.M., van Hulten, M., Jeandel, C., Severmann, S., Tagliabue, A., 2016. Quantifying trace element and isotope fluxes at the ocean–sediment boundary: a review. Phil. Trans. R. Soc. A: Math. Phys. Eng. Sci. 374.
- Homoky, W.B., Conway, T.M., John, S.G., König, D., Deng, F., Tagliabue, A., Mills, R.A., 2021. Iron colloids dominate sedimentary supply to the ocean interior. Proc. Natl. Acad. Sci. 118 e2016078118.
- Jahnke, R., Richards, M., Nelson, J., Robertson, C., Rao, A., Jahnke, D., 2005. Organic matter remineralization and porewater exchange rates in permeable South Atlantic bight continental shelf sediments. Cont. Shelf Res. 25, 1433–1452.

- John, S.G., Mendez, J., Moffett, J., Adkins, J., 2012. The flux of iron and iron isotopes from San Pedro Basin sediments. Geochim. Cosmochim. Acta 93, 14–29.
- Jones, M.E., Beckler, J.S., Taillefert, M., 2011. The flux of soluble organic-iron(III) complexes from sediments represents a source of stable iron(III) to estuarine waters and to the continental shelf. Limnol. Oceanogr. 56, 1811–1823.
- Krauskopf, K.B., 1957. Separation of manganese from iron in sedimentary processes. Geochim. Cosmochim. Acta 12, 61–84.
- Lenstra, W.K., Hermans, M., Séguret, M.J.M., Witbaard, R., Severmann, S., Behrends, T., Slomp, C.P., 2021. Coastal hypoxia and eutrophication as key controls on benthic release and water column dynamics of iron and manganese. Limnol. Oceanogr. 66, 807–826.
- Lohan, M.C., Bruland, K.W., 2008. Elevated Fe(II) and dissolved Fe in hypoxic shelf waters off Oregon and Washington: an enhanced source of Iron to coastal upwelling regimes. Environ. Sci. Technol. 42, 6462–6468.
- Lyons, T.W., Severmann, S., 2006. A critical look at iron paleoredox proxies: new insights from modern euxinic marine basins. Geochim. Cosmochim. Acta 70, 5698–5722.
- Matsui, G.Y., Volkenborn, N., Polerecky, L., Henne, U., Wethey, D.S., Lovell, C.R., Woodin, S.A., 2011. Mechanical imitation of bidirectional bioadvection in aquatic sediments. Limnol. Oceanograph. Methods 9, 84–96.
- Millero, F.J., Sotolongo, S., Izaguirre, M., 1987. The oxidation-kinetics of Fe(II) in seawater. Geochim. Cosmochim. Acta 51, 793–801.
- Murray, J.W., Gill, G., 1978. Geochemistry of iron in puget sound. Geochim. Cosmochim. Acta 42, 9–19.
- Nielsen, L.P., Risgaard-Petersen, N., 2015. Rethinking sediment biogeochemistry after the discovery of electric currents. Annu. Rev. Mar. Sci. 7, 425–442.
- Pham, A.N., Waite, T.D., 2008. Oxygenation of Fe(II) in natural waters revisited: Kinetic modeling approaches, rate constant estimation and importance of various reaction pathways. Geochim. Cosmochim. Acta 72, 3616–3630.
- Raiswell, R., Anderson, T.F., 2005. Reactive iron enrichment in sediments deposited beneath euxinic bottom waters: constraints on supply by shelf recycling. Geol. Soc. Lond., Spec. Publ. 248, 179–194.
- Raiswell, R., Canfield, D.E., 2012. The Iron biogeochemical cycle past and present. Geochem. Perspect. 1. 1–220.
- Reimers, C.E., Jahnke, R.A., Thomsen, L., 2001. In situ sampling in the benthic boundary layer. In: Boudreau, B.P., Jorgensen, B.B. (Eds.), The Benthic Boundary Layer. Oxford, New York, pp. 245–268.
- Seeberg-Elverfeldt, J., Schluter, M., Feseker, T., Kolling, M., 2005. Rhizon sampling of porewaters near the sediment-water interface of aquatic systems. Limnol. Oceanograph. Methods 3, 361–371.
- Sell, K.S., Morse, J.W., 2006. Dissolved Fe²⁺ and ΣH₂S behavior in sediments seasonally overlain by hypoxic to anoxic waters as determined by CSV microelectrodes. Aquat. Geochem. 12, 179–198.
- Severmann, S., McManus, J., Berelson, W.M., Hammond, D.E., 2010. The continental shelf benthic iron flux and its isotope composition. Geochim. Cosmochim. Acta 74, 3984–4004.
- Shi, X.M., Wei, L., Hong, Q.Q., Liu, L.F., Wang, Y.N., Shi, X.Y., Ye, Y., Cai, P.H., 2019. Large benthic fluxes of dissolved iron in China coastal seas revealed by Ra-224/Th-228 disequilibria. Geochim. Cosmochim. Acta 260, 49–61.
- Song, S., Santos, I.R., Yu, H., Wang, F., Burnett, W.C., Bianchi, T.S., Dong, J., Lian, E., Zhao, B., Mayer, L., Yao, Q., Yu, Z., Xu, B., 2022. A global assessment of the mixed layer in coastal sediments and implications for carbon storage. Nat. Commun. 13, 4903. https://doi.org/10.1038/s41467-022-32650-0.
- Steiner, Z., Lazar, B., Erez, J., Turchyn, A.V., 2018. Comparing Rhizon samplers and centrifugation for pore-water separation in studies of the marine carbonate system in sediments. Limnol. Oceanograph. Methods 16, 828–839.
- Stookey, L.L., 1970. Ferrozine-a new spectrophotometric reagent for iron. Anal. Chem. 42, 779–781.
- Stumm, W., Lee, G.F., 1961. Oxygenation of ferrous Iron. Ind. Eng. Chem. 53, 143–146. Sundby, B., Anderson, L.G., Hall, P.O.J., Iverfeldt, A., Vanderloeff, M.M.R., Westerlund, S.F.G., 1986. The effect of oxygen on release and uptake of cobalt,
 - manganese, iron, and phosphate at the sediment-water interface. Geochim. Cosmochim. Acta 50, 1281–1288.
- Taillefert, M., Bono, A.B., Luther, G.W., 2000. Reactivity of freshly formed Fe(III) in synthetic solutions and (pore)waters: Voltammetric evidence of an aging process. Environ. Sci. Technol. 34, 2169–2177.
- Taillefert, M., Neuhuber, S., Bristow, G., 2007. The effect of tidal forcing on biogeochemical processes in intertidal salt marsh sediments. Geochem. Trans. 8.
 Trans. 8.
- Taylor, R.J., 1987. Manganese Geochemistry in Galveston Bay Sediment. PhD Texas A&M University.
- Tengberg, A., De Bovee, F., Hall, P., Berelson, W., Chadwick, D., Ciceri, G., Crassous, P., Devol, A., Emerson, S., Gage, J., Glud, R., Graziottini, F., Gundersen, J., Hammond, D., Helder, W., Hinga, K., Holby, O., Jahnke, R., Khripounoff, A., Lieberman, S., Nuppenau, V., Pfannkuche, O., Reimers, C., Rowe, G., Sahami, A., Sayles, F., Schurter, M., Smallman, D., Wehrli, B., De Wilde, P., 1995. Benthic chamber and profiling landers in oceanography a review of design, technical solutions and functioning. Prog. Oceanogr. 35, 253-+.
- Thamdrup, B., 2000. Bacterial manganese and iron reduction in aquatic sediments. In: Advances in Microbial Ecology, 16, pp. 41–84.
- Thamdrup, B., Fossing, H., Jørgensen, B.B., 1994. Manganese, iron and sulfur cycling in a coastal marine sediment, Aarhus bay, Denmark. Geochim. Cosmochim. Acta 58, 5115–5129.
- Thibault de Chanvalon, A., Metzger, E., Mouret, A., Knoery, J., Geslin, E., Meysman, F.J. R., 2017. Two dimensional mapping of iron release in marine sediments at submillimetre scale. Mar. Chem. 191, 34–49.

- Ussher, S.J., Worsfold, P.J., Achterberg, E.P., Laes, A., Blain, S., Laan, P., de Baar, H.J.W., 2007. Distribution and redox speciation of dissolved iron on the European continental margin. Limnol. Oceanogr. 52, 2530–2539.
- Viollier, E., Inglett, P.W., Hunter, K., Roychoudhury, A.N., Van Cappellen, P., 2000. The ferrozine method revisited: Fe(II)/Fe(III) determination in natural waters. Appl. Geochem. 15, 785–790.
- Wehrmann, L.M., Formolo, M.J., Owens, J.D., Raiswell, R., Ferdelman, T.G., Riedinger, N., Lyons, T.W., 2014. Iron and manganese speciation and cycling in glacially influenced high-latitude fjord sediments (West Spitsbergen, Svalbard):
- evidence for a benthic recycling-transport mechanism. Geochim. Cosmochim. Acta $141,\,628-655.$
- Wehrmann, L., Swenson, M., Perger, D.A., Dwyer, I.P., Volkenborn, N., Heilbrun, C., Aller, R.C., 2023. Ideas and perspectives: the benthic iron flux from sandy-advective bioturbated sediments. Biogeosci. Discuss. https://doi.org/10.5194/bg-2022-247 [preprint]. in review, 2023.
- Zhu, Q., Aller, R.C., 2012. Two-dimensional dissolved ferrous iron distributions in marine sediments as revealed by a novel planar optical sensor. Mar. Chem. 136–137, 14–23